Polymer 49 (2008) 3816–3825

Contents lists available at ScienceDirect

Polymer

journal homepage: www.elsevier.com/locate/polymer

Fracture behaviours of in situ silica nanoparticle-filled epoxy at different temperatures

Hui Zhang [a], Long-Cheng Tang [a,b], Zhong Zhang [a,*], Klaus Friedrich [c], Stephan Sprenger [d]

[a] National Center for Nanoscience and Technology, 100190 Beijing, China
[b] Department of Modern Mechanics, University of Science and Technology of China, 230027 Hefei, China
[c] Institute for Composite Materials, University of Kaiserslautern, 67663 Kaiserslautern, Germany
[d] nanoresins AG, 21502 Geesthacht, Germany

ARTICLE INFO

Article history:
Received 21 February 2008
Received in revised form 24 June 2008
Accepted 26 June 2008
Available online 1 July 2008

Keywords:
Nanosilica particles
Epoxy matrix
Fracture toughness

ABSTRACT

Fracture behaviours of nanosilica filled bisphenol-F epoxy resin were systematically investigated at ambient and higher temperatures (23 °C and 80 °C). Formed by a special sol–gel technique, the silica nanoparticles dispersed almost homogenously in the epoxy resin up to 15 vol.%. Stiffness, strength and toughness of epoxy are improved simultaneously. Moreover, enhancement on fracture toughness was much remarkable than that of stiffness. The fracture surfaces taken from different test conditions were observed for exploring the fracture mechanisms. A strong particle–matrix adhesion was found by fractography analysis. The radius of the local plastic deformation zone calculated by Irwin model was relative to the increment in fracture energy at both test temperatures. This result suggested that the local plastic deformation likely played a key role in toughening of epoxy.

© 2008 Elsevier Ltd. All rights reserved.

1. Introduction

Homogeneous and non-agglomerate dispersion of nanofillers in polymers is a major challenge for fabricating polymeric nanocomposites, especially when an attempt of scale-up the dispersing processes from laboratory to industrial level is favored [1]. Due to lower expense and compatibility to the subsistent industrial equipments, the mechanical mixing, i.e. directly introducing nanofiller powder to polymers, becomes one of the most commonly used processing approaches nowadays. Unfortunately, numerous works have found that the traditional mechanical mixing has a great difficulty in the preparation of agglomerate-free nanocomposites. Addition of high loading nanofillers dramatically increases the viscosity of polymer mixture, which hinders its subsequent compounding with fibers using impregnation processes, e.g. resin transfer moulding. Moreover, the micrometer and submicrometer agglomerates in nanocomposites often exert adverse effects on the mechanical properties of pristine polymers, counteract the positive effects of nanofillers. Accordingly, the results obtained from this kind of composites do not represent the properties of real nanocomposites and even lead to some misunderstanding in nanocomposite researches.

In comparison with the mechanical mixing methods, the sol–gel technique introducing nanofillers into pre-polymers by chemical reaction has been proved to be effective in fabricating agglomerate-free nanocomposites [2,3]. With the development of this technique, colloidal nanosilica sols in epoxy resins or acrylate monomers can be commercially produced in large quantities [4]. Owing to the uniform dispersion, narrow size distribution and quasi-spheral shape of nanosilica, the composites prepared may serve as an ideal model material for investigating the structure–property relationship of nanocomposites. In recent years several works have been focused on this kind of sol–gel-formed nanosilica/polymer systems [5–10]. As reinforcements, silica nanoparticles simultaneously improved the elastic modulus, fracture toughness and scratch resistance of polymers without significantly thickening the matrices [3,11]. The enhanced mechanical properties appeared did not attenuate when nanosilica loading was up to 50 wt.% [2]. The silica nanoparticles also caused a much smaller viscosity increase of polymer systems, as compared to the preformed fumed silica [3]. A small amount of silica nanoparticles can modify the adhesion property of rubber-modified epoxy adhesive [5]; in particular, they exhibited a synergistic effect with reactive liquid rubber in toughening epoxy resin [6]. More recently, it was found based on TEM images together with other thermomechanical analyses that the silica nanoparticles shifted the resin/hardener ratio, forming a core–shell structure, which influenced the matrix physicochemical properties to some degree [8]. This finding, from a certain angle, supported our previous hypothesis that with reduction of

* Corresponding author. National Center for Nanoscience and Technology, No. 11 Beiyitiao Zhongguancun, Beijing 100190, China. Tel./fax: +86 10 82545586.
E-mail address: zhong.zhang@nanoctr.cn (Z. Zhang).

0032-3861/$ – see front matter © 2008 Elsevier Ltd. All rights reserved.
doi:10.1016/j.polymer.2008.06.040

Table 1
Mechanical properties of bisphenol-F epoxy nanocomposites

Nanosilica content [vol.%]	Temperature [°C]	Tension property				Microhardness [MPa]	Impact energy [kJ/m^2]	K_{IC} [MPa m$^{1/2}$]	G_{IC} [J/m^2]
		E [GPa]	σ_y [MPa]	σ_B [MPa]	ε_B [%]				
0	23	3.02 ± 0.20	82.39 ± 1.25	78.98 ± 3.55	4.85 ± 0.75	176.58 ± 1.18	33.70 ± 3.70	0.64 ± 0.07	118.50
	80	2.78 ± 0.01	57.60 ± 0.81	44.09 ± 3.41	5.14 ± 0.65	–	–	0.56 ± 0.04	100.20
1	23	3.22 ± 0.02	82.94 ± 0.50	78.55 ± 3.74	4.98 ± 0.26	180.50 ± 2.45	48.33 ± 1.52	0.65 ± 0.04	115.42
	80	2.90 ± 0.06	59.37 ± 0.14	48.39 ± 5.73	4.36 ± 0.70	–	–	0.64 ± 0.04	122.06
3	23	3.29 ± 0.08	82.43 ± 1.31	78.10 ± 3.68	4.11 ± 0.59	186.39 ± 2.75	49.09 ± 7.67	0.78 ± 0.04	160.57
	80	2.91 ± 0.09	59.72 ± 0.75	45.78 ± 2.21	4.10 ± 0.54	–	–	0.75 ± 0.08	168.63
6	23	3.49 ± 0.03	83.88 ± 1.13	76.15 ± 4.36	3.89 ± 0.39	194.24 ± 6.28	45.27 ± 1.99	0.85 ± 0.02	182.94
	80	3.25 ± 0.03	59.71 ± 0.04	44.61 ± 2.62	4.70 ± 1.21	–	–	0.90 ± 0.07	217.05
7	23	3.67 ± 0.08	83.92 ± 0.83	75.53 ± 3.87	3.83 ± 0.06	194.24 ± 2.55	52.57 ± 4.49	0.89 ± 0.03	189.33
	80	3.19 ± 0.03	60.27 ± 0.23	45.33 ± 3.07	3.91 ± 0.34	–	–	0.99 ± 0.04	267.88
8	23	3.60 ± 0.06	83.80 ± 2.41	78.87 ± 3.32	2.97 ± 0.37	199.14 ± 3.53	42.97 ± 8.24	0.92 ± 0.03	204.97
	80	3.36 ± 0.07	60.68 ± 0.56	48.15 ± 2.79	4.57 ± 1.22	–	–	1.04 ± 0.07	281.75
10	23	3.92 ± 0.11	85.90 ± 0.64	74.65 ± 3.11	3.98 ± 0.06	202.09 ± 4.32	54.78 ± 2.36	0.99 ± 0.03	217.34
	80	3.43 ± 0.07	59.12 ± 0.11	43.81 ± 1.38	4.57 ± 1.34	–	–	1.10 ± 0.08	307.78
13	23	4.13 ± 0.01	83.37 ± 3.99	80.33 ± 2.84	2.99 ± 0.76	214.84 ± 2.35	35.79 ± 8.65	1.03 ± 0.04	225.27
	80	3.73 ± 0.08	59.79 ± 1.04	53.23 ± 6.09	3.00 ± 0.79	–	–	1.12 ± 0.09	295.89
15	23	4.47 ± 0.05	88.94 ± 0.68	82.76 ± 4.21	3.03 ± 0.41	217.78 ± 2.16	43.66 ± 2.76	1.13 ± 0.03	252.95
	80	3.98 ± 0.19	59.18 ± 0.99	45.02 ± 1.26	8.04 ± 3.74	–	–	1.26 ± 0.03	348.15

interparticle distance, the interphase around nanoparticles may construct a three-dimensional physical network dominating the performance of nanocomposites [11].

On the other hand, although sol–gel-formed silica nanoparticles have been reported to toughen different epoxy systems effectively, their toughening mechanisms (i.e. failure modes) have not yet been clear. Various mechanisms have been proposed in literatures, e.g. crack deflection [7], particle debonding and subsequent void growth [9], yielded zone and nano-voids development [10]. These failure modes may occur simultaneously, interplaying with each other and contributing the fracture toughness more or less. Furthermore, the dependency of the type of matrix used and test conditions applied should be considered. It is believed that further elaborate experiments are still needed to deeply understand the toughening phenomena.

In the present work we have chosen a 40 wt.% nanosilica/epoxy masterbatch for preparing a series of epoxy-based nanocomposites with various nanosilica loadings. The major objective is to understand the dependence of fracture behaviours on the nanoparticle loading and test temperatures. Moreover, the toughening mechanisms were discussed, supported by fractography analysis and modeling attempts.

2. Experimental

2.1. Materials and preparation

We chose a bisphenol-F epoxy resin as a matrix (specific equivalent weight of 172 g/equiv). Its K_{IC} value was about 0.64 MPa m$^{1/2}$ (Table 1). A bisphenol-F epoxy masterbatch containing about 40 wt.% of silica nanoparticles (Nanopox F520, specific equivalent weight of 275 g/equiv), and an acid anhydride curing agent (Albidur HE600, specific equivalent weight of 170 g/equiv) were supplied by nanoresins AG, Germany. Silica nanoparticles were formed in situ by a special sol–gel technique. Fig. 1 shows that the nanosilica (8 vol.%) dispersed in the epoxy resin in the form of separated individual spheres. Actually, the agglomerate-free composites can be obtained even at nanosilica loading up to 15 vol.%. The average diameter of silica nanoparticles was about 25 nm measured with TEM. The samples were designated as 'Fx', where 'F' means bisphenol-F epoxy matrix, and 'x' represents the volume fraction of nanosilica in this sample (Table 1). For example, 'F8' means a bisphenol-F epoxy sample containing about 8 vol.% nanosilica particles.

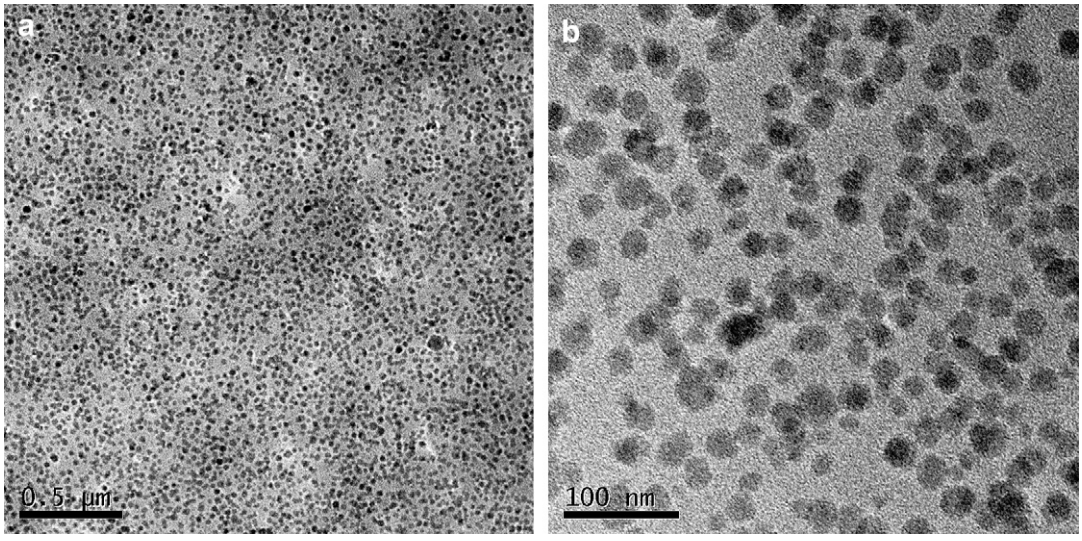

Fig. 1. Transmission electron microscopy (TEM) micrographs taken from epoxy-based nanocomposites with 8 vol.% silica nanoparticles: (a) lower magnification and (b) higher magnification.

Epoxy-based nanocomposites were prepared by mixing the masterbatch with an appropriate amount of the neat epoxy resin and a stoichiometric ratio of the curing agent (which was calculated according to the equivalent weight values of the materials used). The mixture was degassed in a vacuum oven and then cast into release-agent-coated aluminium moulds. The curing schedule used in this work was: 120 °C for 1 h followed by 160 °C for 2 h, as suggested by the supplier. As a result, a series of nanocomposites with various silica contents ranging from 1 vol.% to 15 vol.% were obtained.

2.2. Property investigations

Mechanical and thermal properties of nanocomposites were systematically studied in this work, which consisted of tensile test, microhardness, unnotched Charpy impact, dynamic mechanical thermal analysis (DMTA) and quasi-static fracture test. The tensile and quasi-static fracture tests were also carried out at 80 °C as well. Glass transition temperature, T_g, of the nanocomposites was obtained via both DMTA and differential scanning calorimetry (DSC). The detailed experimental procedures were described elsewhere [11]. It should be noted that for the quasi-static fracture test, dimensions of the compact tension (CT) specimen applied here were $5.7 \times 36 \times 36\ mm^3$ (thickness × length × width), a crosshead speed of 1 mm/min was used at both test temperatures.

The quality of nanoparticle dispersion was first observed under a transmission electron microscope (TEM, FEI Tecnai G20). Fracture surfaces of the materials studied after mechanical tests were examined by an optical microscope and a scanning electron microscope (SEM, JEOL 5400). Prior to SEM observation, the fracture surfaces were sputtered with Pt/Pd alloy for about 150 s.

To make a quantitative characterization of fracture surface of CT specimen, the three-dimensional topographs were scanned by a laserprofilometer (UBM Messtechnik). The surface roughness was subsequently determined in terms of arithmetic average surface roughness, R_a, and square root average surface roughness, R_q, according to DIN 4768. At least five scans at different positions near crack initiation region of each specimen were taken in order to achieve better accuracy.

3. Results and discussion

3.1. Glass transition temperature

Fig. 2 presents the glass transition temperature (T_g) of the bisphenol-F nanocomposites, measured by both DSC and DMTA techniques. Note that for a given material, T_g value measured via DMTA is not identical to that via DSC. It is ascribed to the different measuring principles of two techniques. It can be seen that the T_g values gradually declined with nanosilica content. According to the DSC results, T_g value dropped by about 18 °C at nanoparticle content of 15 vol.%. The decline in T_g has also been found in other nanoparticle-filled thermoplastic and thermosetting polymer systems [12–18], and its origin has not been clearly understood. Several assumptions have been proposed for interpreting this phenomenon, e.g. the plasticizing effect of uncured epoxy resin [12–14], the influence of absorbed moisture or residual organics [15], the extra free volume at nanofiller–resin interface [16], the weak filler–resin adhesion [17], as well as the effect of ultra-thin film [18]. In this work it is difficult for us to determine which reason is responsible for the decline in T_g, but it is easily understood that the reduced T_g reflects the enhanced mobility of polymer segment, which probably be of help to toughen the epoxy resin.

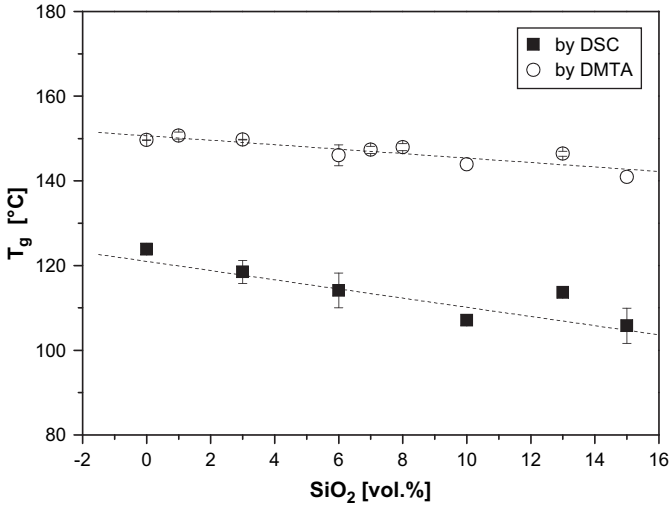

Fig. 2. Glass transition temperature of silica/epoxy nanocomposites as a function of silica nanoparticle volume content.

3.2. Mechanical properties

The basic mechanical properties of the bisphenol-F nanocomposites were thoroughly investigated at room temperature. Some of the tests were also undertaken at 80 °C. The results are summarized in Table 1. The present results are quite in agreement with our previous results [11], which will be not discussed in detail in this paper. The general tendency is that the incorporation of nanosilica particles increased effectively the elastic modulus, microhardness of epoxy matrix. It also improved the Charpy impact resistance of matrix at lower filler content, whereas it did not affect the yielding stress, ultimate fracture stress and strain at break at all. With regard to the temperature effect, the elastic modulus, yielding stress and ultimate fracture stress were all reduced at elevated test temperature, irrespective of the presence of nanoparticles.

Fig. 3 shows the typical CT curves of epoxy nanocomposites tested at 23 °C and 80 °C. A majority of filled and unfilled epoxy samples exhibit unstable stick-slip crack propagation at both test temperatures. The stick-slip phenomenon is often observed in epoxy resins [19,20] and sometimes in thermoplastic polymer composites [21,22]. Despite some debates in the literature, origin

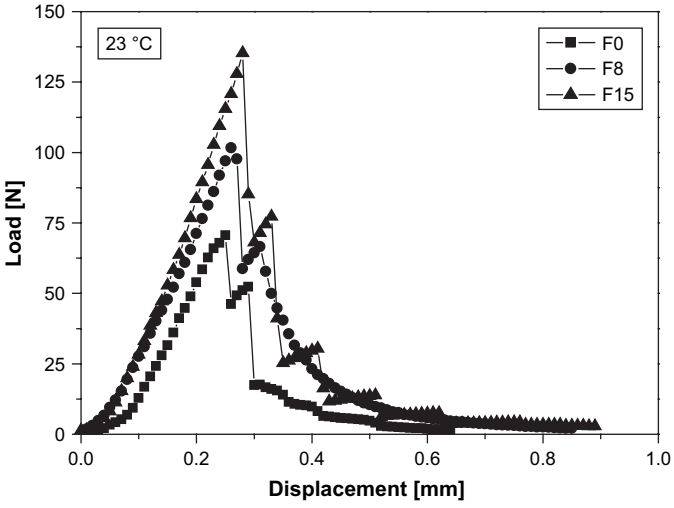

Fig. 3. Typical load–displacement curves of silica/epoxy nanocomposites measured at 23 °C.

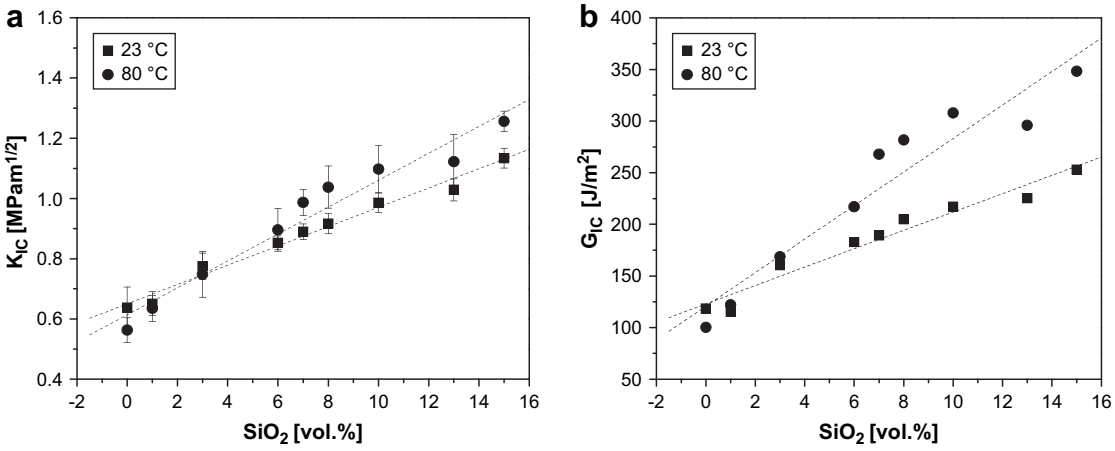

Fig. 4. Fracture toughness of silica/epoxy nanocomposites at 23 °C and 80 °C: (a) K_{IC} and (b) G_{IC}.

of stick-slip crack growth is commonly explained as the crack tip blunting mechanism [23], which caused by the local plastic flow. Therefore, the factors that facilitate the development of plastic deformation around the crack tip favor the stick-slip behaviors, e.g. the high test temperature or the low strain rate. It is worth to note that the nanocomposites show more obvious stick-slip behaviour than the neat resin. This implies that the higher level of plastic deformation occurred around the crack tip of the nanocomposites.

The fracture toughness of bisphenol-F epoxy nanocomposites is characterized by K_{IC} and G_{IC}, the values of which *vs.* nanosilica volume content at 23 °C and 80 °C are given in Fig. 4. Both K_{IC} and G_{IC} show approximately linear increase with particle content. Due to the agglomerate-free nanocomposite system used here, it is safe to say that nanoparticles improve the fracture toughness of epoxy matrix substantially.

3.3. Fractography

3.3.1. Tensile test

The topography of the fracture surfaces of the epoxy-based nanocomposites is of particular interest. Fig. 5 shows the fractographs taken from tensile tests at room temperature. The fracture surface can be roughly divided into two distinct regions: crack

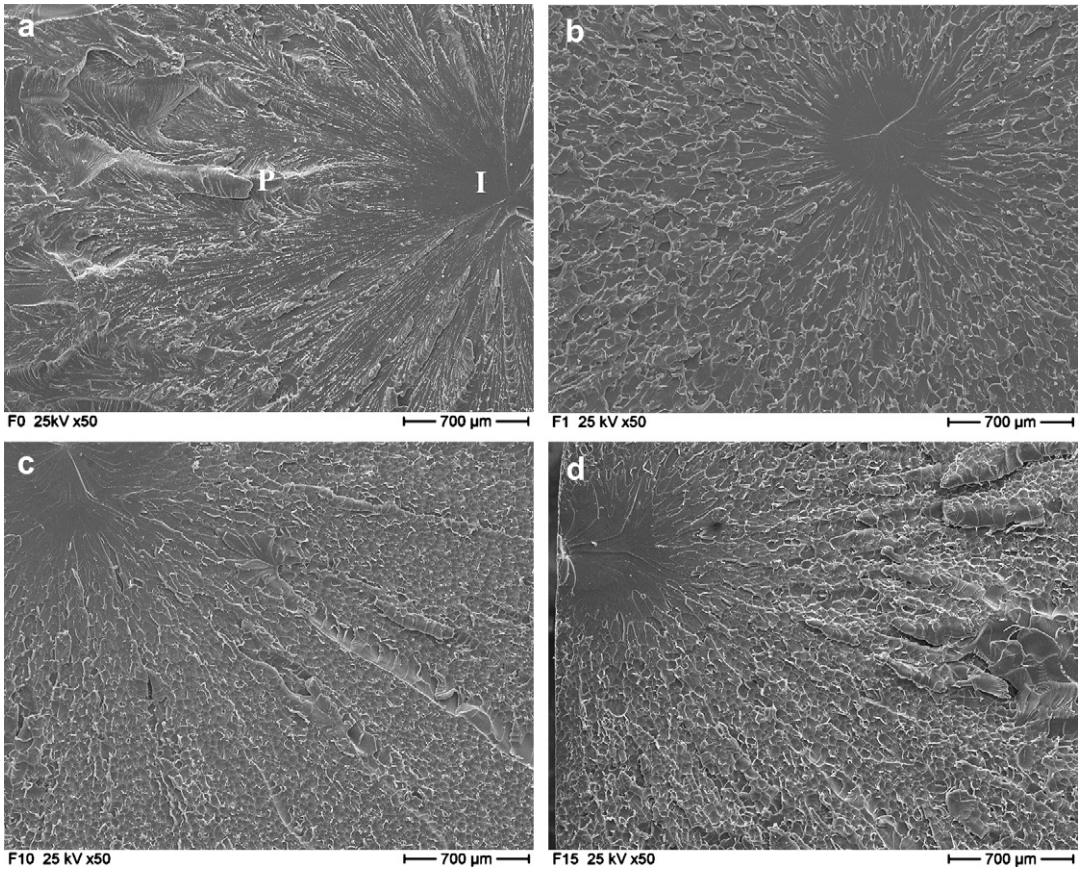

Fig. 5. Lower magnification of SEM fracture surfaces taken from tensile specimens of silica/epoxy nanocomposites measured at 23 °C: (a) neat epoxy, (b) 1 vol.%, (c) 10 vol.% and (d) 15 vol.%.

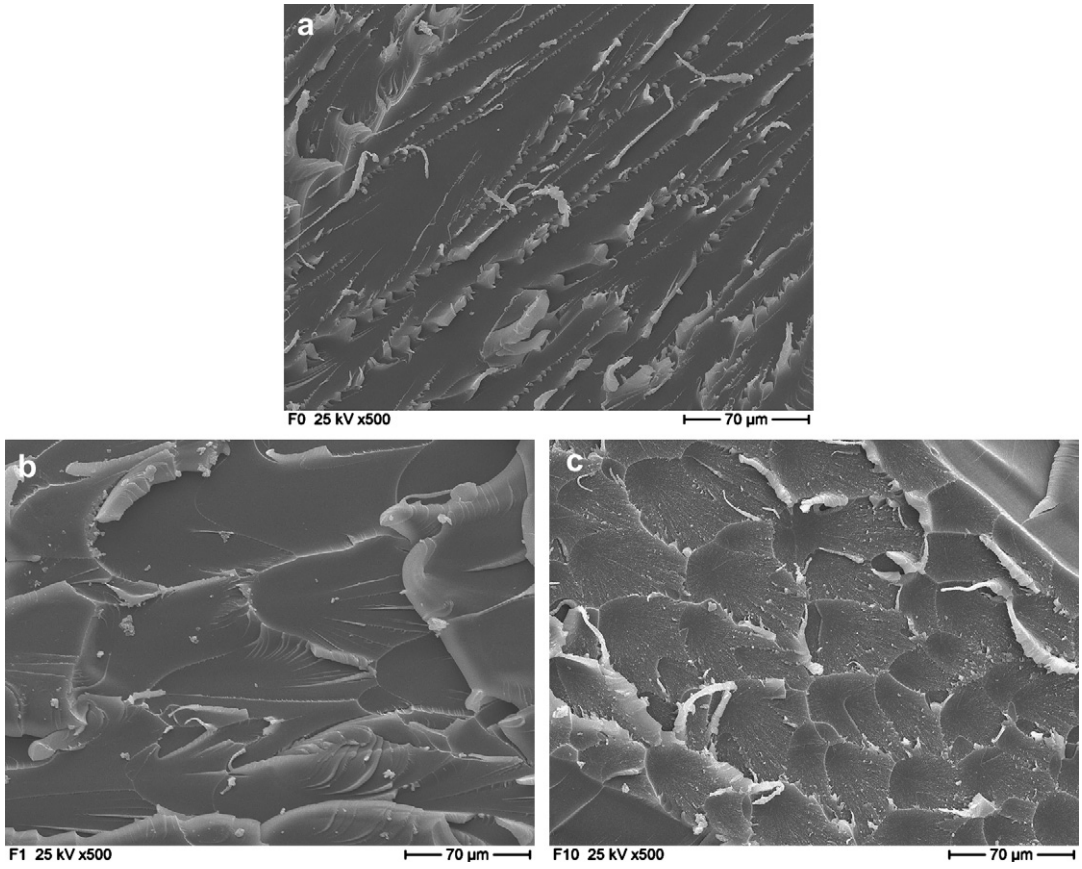

Fig. 6. Higher magnification of SEM fracture surfaces taken from tensile specimens of silica/epoxy nanocomposites measured at 23 °C: (a) neat epoxy, (b) 1 vol.%, (c) 10 vol.%.

initiation zone and crack propagation zone (indicated by 'I' and 'P', respectively, in Fig. 5a). The former looks dark grey in SEM images and is distinguished by a relatively smooth area together with several river markings indicative of cracks propagation occurring on slightly different planes. Surrounding the crack initiation zone is the crack propagation zone, characteristic of very rough surface having hackles or ribbons emanating radially from the initiation site with numerous fracture steps in between. The smooth region usually corresponds to a zone of sub-critical crack growth or a zone over which the crack is accelerating, while the rough region relates to a very fast fracture zone, formed due to the considerable branching of the primary crack [24]. Fig. 5 shows that at room temperature the size of the smooth region of the unfilled epoxy material is roughly the same as that of the filled material. However, the appearance of the rough regions of filled and unfilled materials is disparate. This can be clearly observed in higher magnified SEM images shown in Fig. 6. Numerous dimples are present in the fracture surface of the nanoparticle-filled epoxy resin, and the dimple density increases with particle content. In contrast, there are only ribbons and river lines in the unfilled resin. The formation of the dimples is accompanied by the creation of new fracture surfaces, and thus much fracture energy is likely dissipated. Occasionally, holes can be found in the middle of the dimples, as indicated by a white arrow in Fig. 7. The diameter of the hole is much larger than that of a single particle, implying particle debonding may occur within matrix rather than at particle–matrix interface. This phenomenon suggests that the particle–matrix interfacial adhesion is indeed strong. This is probably because that the silica nanoparticles were beforehand surface-modified with silane coupling agent, which can react with both inorganic particles and epoxy resin and yield strong interfacial adhesion. Further, the debonding process depends strongly on particle size. As particle size decreases, the critical stress necessary to cause debonding increases, resulting in greater difficulty in debonding [25]. The strong interfacial adhesion is additionally supported by Fig. 8, where the majority of silica nanoparticles are embedded in epoxy resin and coated well with epoxy layers, and as a result, the diameter of particles (~70 nm, Fig. 8) is much higher than its original

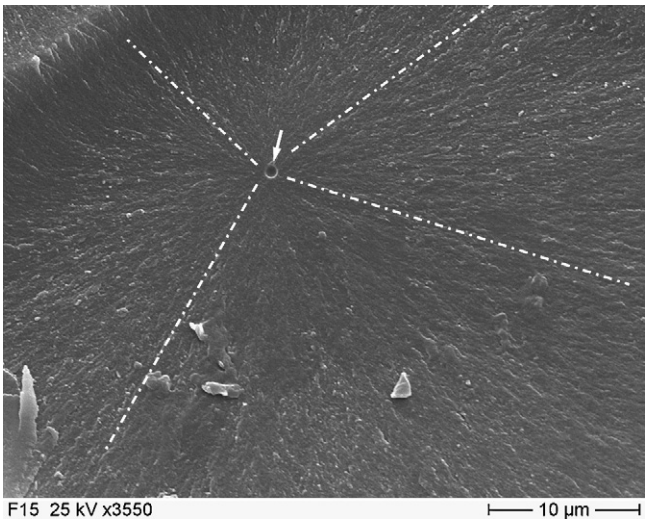

Fig. 7. A close-up of a dimple of silica/epoxy nanocomposite taken from a tensile specimen measured at 23 °C. The arrow indicates cohesive fracture. The silica nanoparticle content is 15 vol.%.

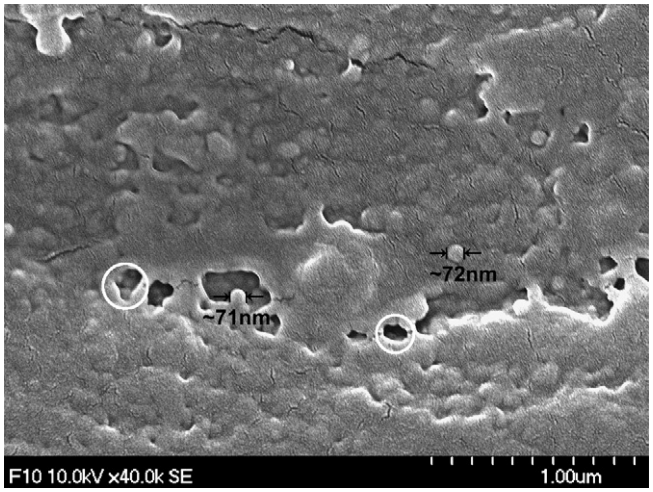

Fig. 8. Higher magnification of SEM fracture surfaces taken from a CT specimen of 10 vol.% silica/epoxy nanocomposites. Some voids after nanoparticle debonding are marked by circles.

average size of 25 nm. Some voids can be still observed on the fracture surface, which may result from the particle debonding. The size of these voids is also greater than the mean diameter of single particle (as marked by circles in Fig. 8). Similar to Fig. 7, the debonding may occur somewhere within matrix.

When the test temperature is increased up to 80 °C the fractographs change markedly, as shown in Fig. 9. The most striking feature is that the smooth zone is significantly larger than that at 23 °C. More notably, the size of the smooth region is associated with nanoparticle content. At higher particle contents the smooth region covers nearly the entire fracture surface, and a few parabolic steps remain on the edge of the fracture surface. The smooth region, as stated earlier, represents a zone of slower fracture [24]. Hence, this morphology of fracture surfaces implies that the higher concentration nanoparticles can effectively hinder fast crack growth and therefore help to prevent earlier catastrophic fracture of materials on loading.

In addition, it is also seen from Fig. 7 that basic longitudinal texture (BLT, the finest texture formed on the fracture surface [26], as guided by some dash lines) emanates radially from the hole of the dimple. Since the BLT is parallel to the direction of local crack propagation [27], this morphology suggests that the direction of local cracks is not always the same as that of macroscopic crack propagation. Based on the above discussion, it can be concluded that the presence of nanoparticles can influence the fracture behaviours of epoxy matrix at both microscopic and macroscopic scales.

3.3.2. Compact tension test

Fig. 10 presents an overview of the CT fractographs of the neat epoxy resin and the nanocomposites. The figure is a collage of eight optical micrographs taken from the CT fracture surface. Clearly, the fracture surface becomes rougher after the addition of nanosilica particles. SEM micrographs offer an insight into the fracture behaviour of unfilled and filled epoxy resins. Fig. 11 shows the SEM fractographs taken near the crack tip of CT specimens tested at room temperature. Neat epoxy resin has a mirror-smooth fracture surface (Fig. 11a), whereas nanocomposites possess a fracture surface with numerous river-like lines (Fig. 11b). Elevated test temperature results in softening and trace of plastic flow of the

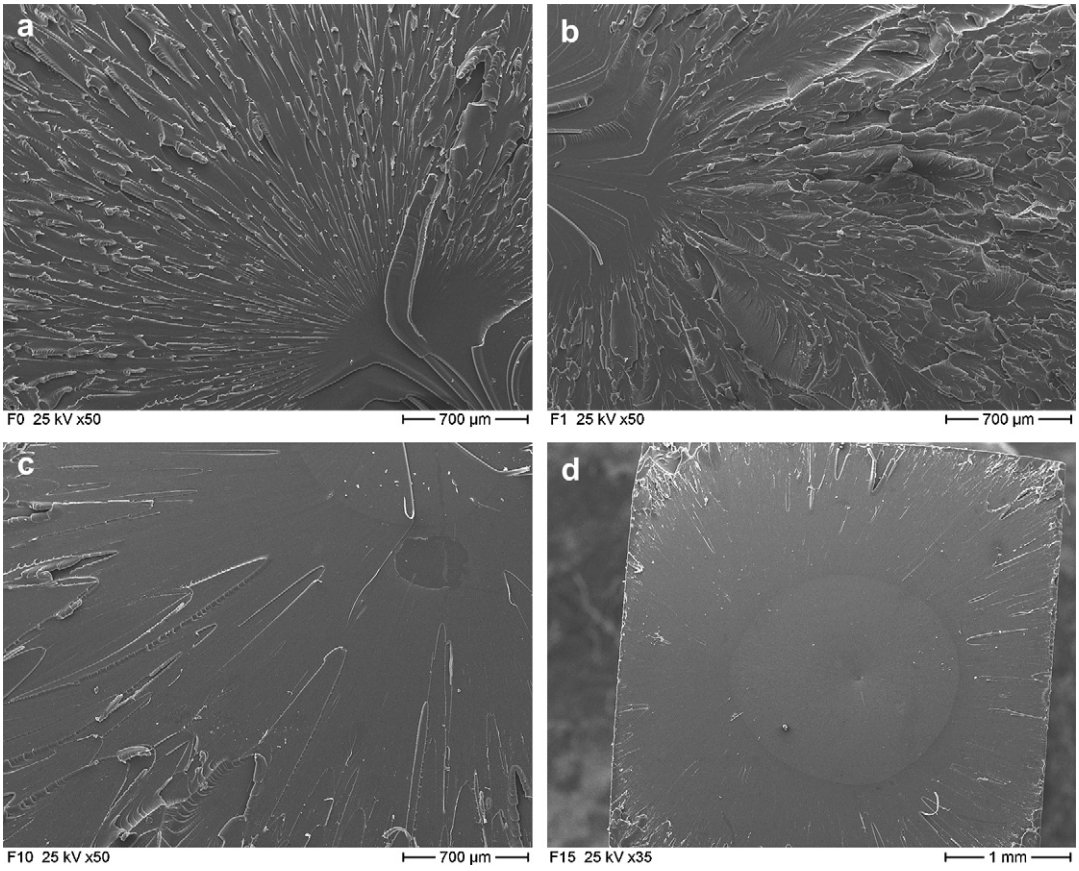

Fig. 9. Lower magnification of SEM fracture surfaces taken from tensile specimens of silica/epoxy nanocomposites measured at 80 °C: (a) neat epoxy, (b) 1 vol.%, (c) 10 vol.% and (d) 15 vol.%.

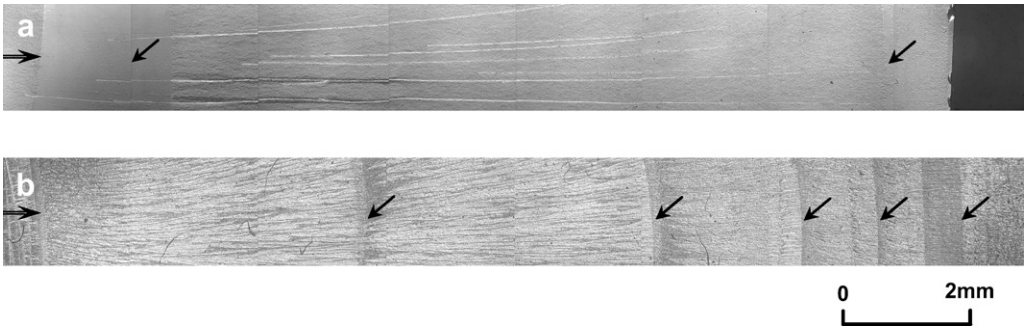

Fig. 10. Overview of CT fracture surfaces measured by optical microscope at room temperature: (a) neat matrix, (b) 15 vol.% silica nanoparticles. The horizontal arrow indicates the crack initiation site, and the arrow at 45° angle indicates the arrest lines.

nanocomposites (Fig. 11c), however, the fracture surface is still featureless in the case of the neat epoxy resin (not shown here).

Laserprofilometry provides an approach to quantitatively characterize the 3D appearance of the CT fracture surface. Typical topographies of the CT samples are shown in Fig. 12. The array of parallel ridges in this figure represents the river lines shown in SEM micrographs. Similarly, the river lines tend to be deflected and thus yielding a very rough surface at higher filler content. The arithmetic surface roughness, R_a, and the square root surface roughness, R_q develop similar tendency, as shown in Fig. 13. The test temperature appears to have no significant effect on the surface roughness of materials studied. Despite some scatter of the experimental data, the surface roughness rises dramatically at lower filler content, and then reaches a plateau at higher filler content.

3.4. Toughening mechanisms

Various toughening mechanisms have been proposed to explain the complicated toughening phenomena of the rigid particle filled polymer systems, which include (a) crack deflection, (b) crack branching, (c) crack pinning/bowing, (d) particle bridging, (e) particle debonding, (f) micro-cracking or crazing of matrix, and (g) inelastic deformation of matrix. Among these mechanisms, the items (a)–(d) are termed as 'on-fracture plane process', since these processes take place on or in the immediate vicinity of the fracture surface. Comparatively, those processes occurring below the fracture surface (around the crack tip) are designated as 'off-fracture plane process', such as items (e)–(g). On- and off-fracture plane processes usually occur simultaneously and contribute to the

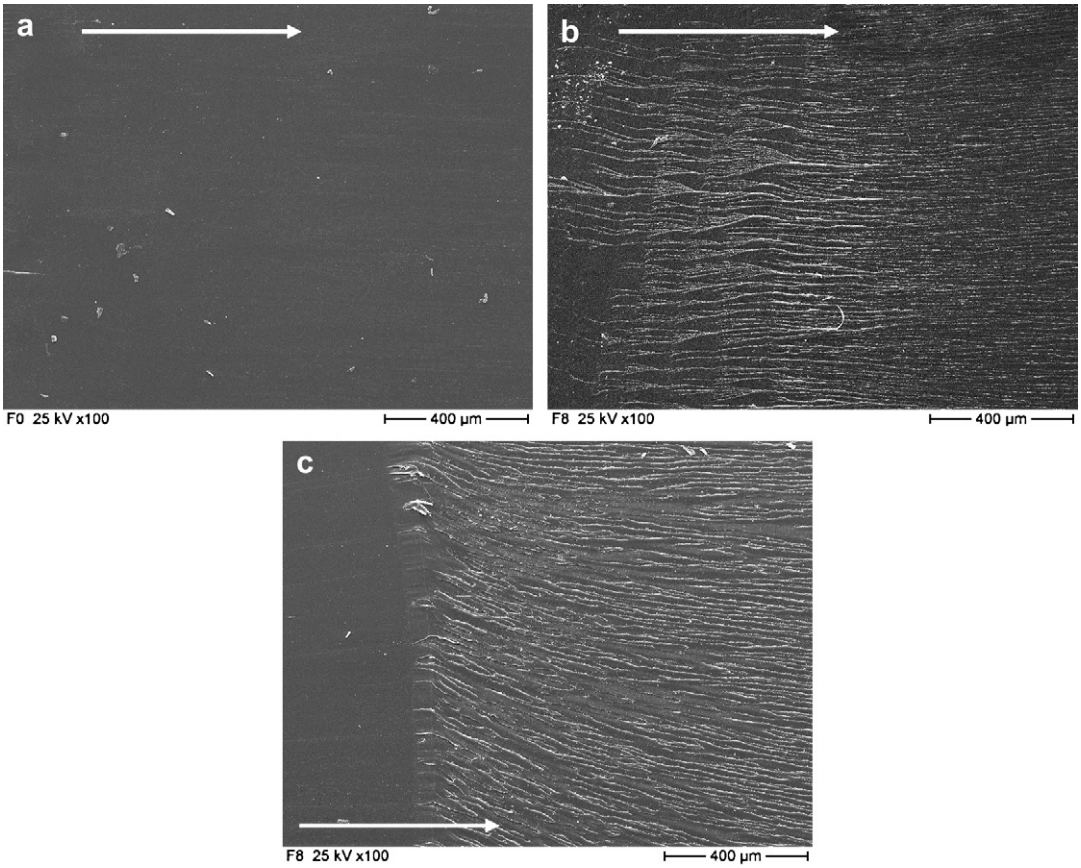

Fig. 11. SEM fracture surfaces taken from CT specimens: (a) neat epoxy measured at 23 °C, (b) 8 vol.% silica nanoparticles, measured at 23 °C and 8 vol.% silica nanoparticles, measured at 80 °C.

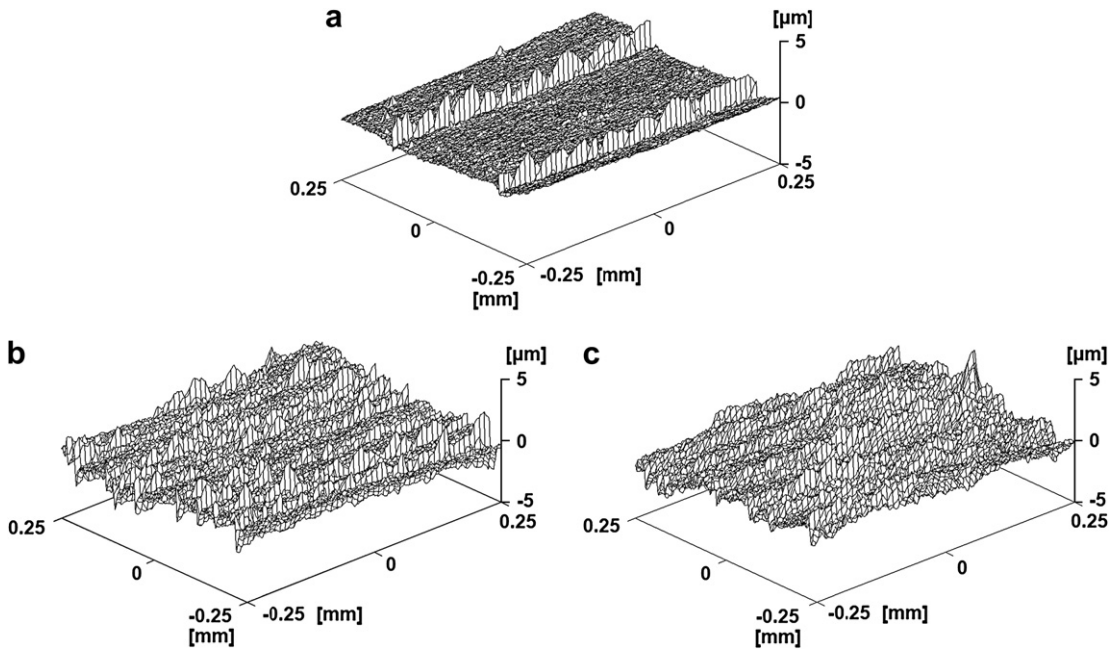

Fig. 12. Typical laserprofilometry topography of silica/epoxy nanocomposites taken from CT samples measured at 23 °C: (a) neat matrix, (b) 10 vol.% silica nanoparticles and (c) 15 vol.% silica nanoparticles.

toughening more or less. Recently, Norman and Robertson [28] found that the increment in fracture energy arose almost completely from off-fracture plane processes for micron-sized rigid-particle/glassy polymer composites. However, as far as we know, there is a lack of the knowledge of nanofiller toughening. In the present work, some mechanisms appear to be active and they are discussed in the following sections.

The crack deflection effect is the first candidate, since it is commonly thought to be an important toughening mechanism of micron-sized rigid particle filled polymers. The crack deflection toughening was introduced by Farber and Evans [29,30]. According to this assumption, when a crack front approaches an obstacle, it is tilted and even twisted out of its original plane. This alters the stress state near crack tip, produces non-planar cracks, increases fracture surface roughness, and in turn consumes additional fracture energy. With respect to our nanocomposites, SEM and OM micrographs of CT specimens show the tortuous crack trajectories (Figs. 10b and 11b), as compared to the straight cracks of neat epoxy resin (Figs. 10a and 11a). Also, addition of nanoparticles results in much rougher (i.e. additional) fracture surfaces as examined via the laserprofilometer (Figs. 12 and 13). These experimental observations seem to accord with the features of crack deflection effect. In order to verify whether it indeed operates in the nanocomposites and how much it contributes to the dissipation of fracture energy, an analytical model [31] that describes the increment of fracture energy, ΔG, due to the crack deflection effect was used:

$$\Delta G = 3\gamma_m V_p/2 \tag{1}$$

where, V_p is the volume fraction of particles in the filled material; γ_m is the specific fracture energy of matrix [31]. For particle-filled epoxy resins, the γ_m can be considered as a half of strain energy release rate of matrix [32]. The comparison of ΔG between experimental and model values is shown in Fig. 14. The predicted values, however, failed to fit the experimental values. Combining the fractography analysis mentioned above, we could consider that the crack deflection mechanism only gives minor contribution to the toughening. This may be due to the fact that the nano-sized particles may be too small to deflect the micron-dimensioned crack tip, as reported by Johnsen et al. recently [9].

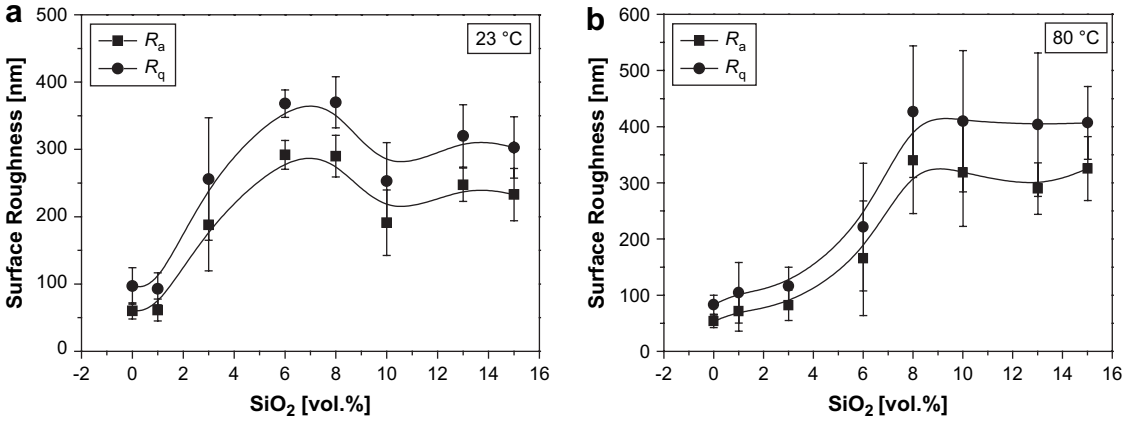

Fig. 13. Surface roughness of CT samples of silica/epoxy nanocomposites as a function of silica nanoparticle volume content, measured at different temperatures: (a) at 23 °C, (b) at 80 °C. R_a and R_p stand for arithmetic surface roughness and square root surface roughness, respectively.

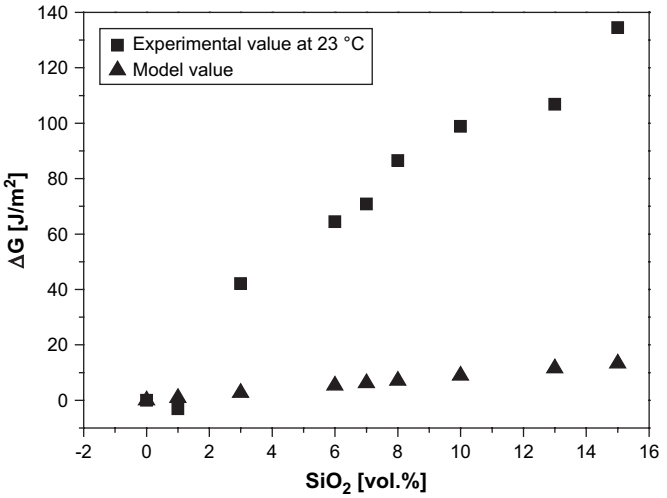

Fig. 14. A comparison of increment in fracture energy between experimental values and model values.

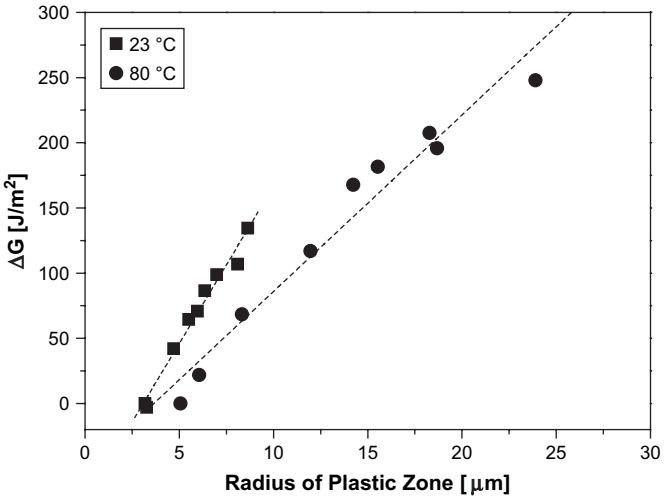

Fig. 16. Correlation between radius of plastic zone and increment of fracture energy of silica/epoxy nanocomposites.

Although highly cured epoxy is known to exhibit high plastic resistance, it can deform and even plastically flow under load. In the current nanocomposite systems, we speculate that the nanoparticles can enhance the plastic deformability around the crack tip, and hence help to consume the fracture energy. There are some evidences that may support this assumption. (1). As mentioned earlier, the filled resins show more stick-slip lines in comparison with the unfilled resin (Fig. 10), the origin of which is usually considered as the local plastic deformation around crack tip. (2). Based on the suggestion of Irwin model [33], the nominal radius of plastic zone, r_P, can be estimated by a relationship (Eq. (2)), if the plane strain state is satisfied.

$$r_P = \frac{1}{6\pi}\left(\frac{K_{IC}}{\sigma_y}\right)^2 \tag{2}$$

where σ_y is the uniaxial yield stress of materials. According to Eq. (2), the radius of plastic zone as a function of nanoparticle volume content is plotted in Fig. 15, where increase of particle volume content enlarges the radius of plastic zone significantly at both test temperatures. (3). A direct evidence has been reported by Ma et al.

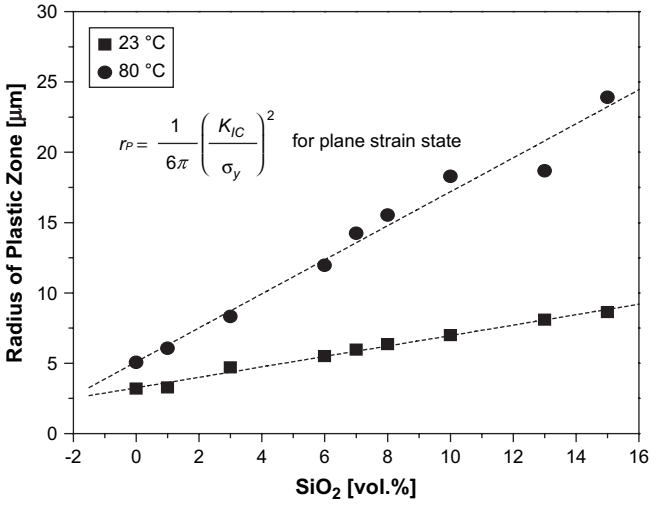

Fig. 15. Effect of silica nanoparticle volume content on radius of nominal plastic zone near crack tip.

[10], where the sol–gel-formed nanosilica/epoxy system is basically similar to the present case. In their study under sub-critical loading, obvious plastic deformation around the crack tip was observed under a polarized optical microscope for the filled epoxy. Additionally, TEM micrographs indicated that along the crack propagation direction, the nanocomposite samples could develop a thin dilatation zone with length of around 1 mm, whereas the neat epoxy samples corresponded to much shorter one (around 6 μm) [10]. It is our opinion that this dilatation zone results from some kind of restricted local yielding, which would be due to the complicated nanoparticle–matrix interactions. In summary, it could be concluded that nanoparticles cause larger *local* plastic deformation around the crack tip, which should be essential for toughening. As additionally proved in Fig. 16, there is a close correlation between the increment of fracture energy and the radius of plastic zone.

However, what is the origin of the enhanced local plastic deformability after addition of nanoparticles? Here, we proposed several possible factors to interpret this phenomenon, although further evidence is still needed to confirm this interpretation. (1). The decline in T_g (Fig. 3) is expected to benefit the mobility of polymer chains and thus leading to relatively higher deformability ahead the crack tip. (2) As given in Fig. 8, despite a strong particle–matrix adhesion, a part of polymer-coated nanoparticles can be still detached from matrix during fracture and thus leaving some voids on the fracture surface. These voids may release the constraint around the crack tip and therefore allow the resin to deform easier [9,28].

4. Conclusions

This paper focused on fracture behaviours of in situ formed nanosilica particle/epoxy composites measured at different test temperatures. Since the nanoparticles were almost homogeneously dispersed in epoxy matrix, the elastic modulus, microhardness, impact resistance as well as fracture toughness of epoxy matrix were simultaneously improved with increasing nanoparticle volume content.

The fractographic analysis confirmed the relatively strong particle–matrix adhesion. It also revealed that nanosilica particles did affect the fracture behaviours of epoxy in various ways at different test temperatures. At room temperature, the addition of nanosilica resulted in numerous dimples, while at higher temperature it caused larger smooth zone on the fracture surfaces and thus decelerating the crack propagation rate. The crack deflection mechanisms of nanoparticles were found to be only minor toughening

effect according to the analytical model. The dominant toughening effect was likely attributable to the enhanced local deformability around the crack tip induced by nanoparticles. This assumption is supported by several items, which include the enhanced stick-slip behaviours, and the reduced T_g, as well as the estimation by Irwin model.

Acknowledgements

This work was partly sponsored by a Key Research Program of the Ministry of Science and Technology of China (Grant No. 2006CB932304) and a Key Item of the Knowledge Innovation Project of Chinese Academy of Sciences (Grant No. KJCX1.YW.07). The authors are grateful to nanoresins AG for the support of nano-SiO_2/epoxy masterbatch.

References

[1] Mackay ME, Tuteja A, Duxbury PM, Hawker CJ, Van Horn B, Guan ZB, et al. General strategies for nanoparticle dispersion. Science 2006;311:1740.
[2] Adebahr T, Roscher C, Adam J. Reinforcing nanoparticles in reactive resins. Eur Coat J 2001;4:144.
[3] Roscher C, Adam J, Eger C, Pyrlik M. Novel radiation curable nanocomposites with outstanding material properties. RadTech02, Tech Conf Proc, Indianapolis; 29 April to 2 May 2002. p. 322–9.
[4] Available from: http://www.nanoresins.de/.
[5] Kinloch AJ, Lee JH, Taylor AC, Sprenger S, Eger C, Egan D. Toughening structural adhesives via nano- and micro-phase inclusions. J Adhes 2003;79:867.
[6] Kinloch AJ, Mohammed RD, Taylor AC, Eger C, Sprenger S, Egan D. The effect of silica nanoparticles and rubber particles on the toughness of multiphase thermosetting epoxy polymers. J Mater Sci 2005;40:5083.
[7] Rosso P, Ye L, Friedrich K, Sprenger S. A toughened epoxy resin by silica nanoparticle reinforcement. J Appl Polym Sci 2006;101:1235.
[8] Rosso P, Ye L. Epoxy/silica nanocomposites: nanoparticle-induced cure kinetics and microstructure. Macromol Rapid Commun 2007;28:121.
[9] Johnsen BB, Kinloch AJ, Mohammed RD, Taylor AC, Sprenger S. Toughening mechanisms of nanoparticle-modified epoxy polymers. Polymer 2007;48:530.
[10] Ma J, Mo M-S, Du X-S, Rosso P, Friedrich K, Kuan H-C. Effect of inorganic nanoparticles on mechanical property, fracture toughness and toughening mechanism of two epoxy systems. doi:10.1016/j.polymer.2008.05.043.
[11] Zhang H, Zhang Z, Friedrich K, Eger C. Property improvements of in situ epoxy nanocomposites with reduced interparticle distance at high nanosilica content. Acta Mater 2006;54:1833.
[12] Ragosta G, Abbate M, Musto P, Scarinzi G, Mascia L. Epoxy–silica particulate nanocomposites: chemical interactions, reinforcement and fracture toughness. Polymer 2005;46:10506.
[13] Becker O, Varley R, Simon G. Morphology, thermal relaxations and mechanical properties of layered silicate nanocomposites based upon high-functionality epoxy resins. Polymer 2002;43:4365.
[14] Liu YL, Hsu CY, Wei WL, Jeng RJ. Preparation and thermal properties of epoxy–silica nanocomposites from nanoscale colloidal silica. Polymer 2003;44:5159.
[15] Preghenella M, Pegoretti A, Migliaresi C. Thermo-mechanical characterization of fumed silica–epoxy nanocomposites. Polymer 2005;46:12065.
[16] Sun YY, Zhang ZQ, Moon KS, Wong CP. Glass transition and relaxation behavior of epoxy nanocomposites. J Polym Sci Part B Polym Phys 2004;42:3849.
[17] Ash BJ, Siegel RW, Schadler LS. Mechanical behavior of alumina/poly(methyl methacrylate) nanocomposites. Macromolecules 2004;37:1358.
[18] Mayes AM. Nanocomposites – softer at the boundary. Nat Mater 2005;4:651.
[19] Spanoudakis J, Young RJ. Crack propagation in a glass particle-filled epoxy resin. Part 1: effect of particle volume fraction and size. J Mater Sci 1984;19:473.
[20] Perkins WG. Polymer toughness and impact resistance. Polym Eng Sci 1999;39:2445.
[21] Ye L, Yuan CT, Mai YW. Effects of rate and temperature on fracture behavior of TPX (poly-4-methyl-1-pentene) polymer. Polym Compos 1998;19:830.
[22] Karger-Kocsis J. Stick-slip type crack growth during instrumented high-speed impact of HDPE and HDPE/SELAR (R) discontinuous laminar microlayer composites. J Macromol Sci Phys 2001;B40:343.
[23] Kinloch AJ, Williams JG. Crack blunting mechanisms in polymers. J Mater Sci 1980;15:987.
[24] Cantwell WJ, Smith JW, Kausch HH. Examination of the processes of deformation and fracture in a silica-filled epoxy resin. J Mater Sci 1990;25:633.
[25] Lee J, Yee AF. Inorganic particle toughening I: micro-mechanical deformations in the fracture of glass bead filled epoxies. Polymer 2001;42:577.
[26] Covavisaruch JS, Robertson RE, Filisko FE. Basic longitudinal texture and fracturing process in thermoset polymers. J Mater Sci 1992;27:990.
[27] Nichols ME, Robertson RE. The toughness of epoxy–poly(butylene terephthalate) blends. J Mater Sci 1994;29:5916.
[28] Norman DA, Robertson RE. Rigid-particle toughening of glassy polymers. Polymer 2003;44:2351.
[29] Farber KT, Evans AG. Crack deflection process-I theory. Acta Metall 1983;31:565.
[30] Farber KT, Evans AG. Crack deflection process-II experiment. Acta Metall 1983;31:577.
[31] Garg AC, Mai YW. Failure mechanisms in toughened epoxy resins – a review. Compos Sci Technol 1988;31:179.
[32] Moloney AC, Kausch HH, Stieger HR. The fracture of particulate-filled epoxide resins. J Mater Sci 1983;18:208.
[33] Kinloch AJ, Young RJ. Fracture behaviour of polymers. London, New York: Applied Science Publishers; 1987. p. 88–93.